Journal of Structural Biology **125,** 209–215 (1999)
Article ID jsbi.1999.4085, available online at http://www.idealibrary.com on IDEAL®

A Strategy for Determining the Orientations of Refractory Particles for Reconstruction from Cryo-Electron Micrographs with Particular Reference to Round, Smooth-Surfaced, Icosahedral Viruses

José R. Castón,*[,1] David M. Belnap,* Alasdair C. Steven,* and Benes L. Trus*[,†,2]

**Laboratory of Structural Biology Research, National Institute of Arthritis, Musculoskeletal and Skin Diseases and †Computational Bioscience and Engineering Laboratory, Center for Information Technology, National Institutes of Health, Bethesda, Maryland 20892-5624*

Received December 10, 1998, and in revised form January 8, 1999

Cryo-electron microscopy and three-dimensional image reconstruction are powerful tools for analyzing icosahedral virus capsids at resolutions that now extend below 1 nm. However, the validity of such density maps depends critically on correct identification of the viewing geometry of each particle in the data set. In some cases—for example, round capsids with low surface relief—it is difficult to identify orientations by conventional application of the two most widely used approaches—"common lines" and model-based iterative refinement. We describe here a strategy for determining the orientations of such refractory specimens. The key step is to determine reliable orientations for a base set of particles. For each particle, a list of candidate orientations is generated by common lines: correct orientations are then identified by computing a single-particle reconstruction for each candidate and then systematically matching their reprojections with the original images by visual criteria and cross-correlation analysis. This base set yields a first-generation reconstruction that is fed into the model-based procedure. This strategy has led to the structural determination of two viruses that, in our hands, resisted solution by other means.

Key Words: **3D reconstruction; capsid structure; common lines.**

INTRODUCTION

All cats look gray in the dark.

—Old Spanish proverb

Icosahedral viruses have played a central role in the development of cryo-electron microscopy (Adrian *et al.*, 1984) and three-dimensional image reconstruction (Baker, 1992; Baker and Johnson, 1997; Chiu, 1993). Their large sizes and distinctive shapes made them readily visible in low-contrast cryo-micrographs and their high order of symmetry facilitated reconstruction, and resolutions below 10Å are now feasible (Conway *et al.*, 1997; Böttcher *et al.*, 1997; Trus *et al.*, 1997). However, for a reconstruction to be valid, the orientation of each capsid must be correctly identified. Moreover, the resolution of the reconstruction is limited by the precision with which the orientation angles are determined, among other factors. Not all viruses are equally tractable in this respect. Capsids with planar facets offer the advantage that their outline varies markedly with viewing direction—hexagonal in a threefold view, pseudo-hexagonal in a twofold view, and round in a fivefold view, whereas spherical capsids appear round from any direction. Capsids with large protrusions project conspicuous features that make them easier to solve than smooth-surfaced capsids, and capsids containing nucleic acids generate noisier images than empty capsids and are less easily solved.

Nowadays, model-based orientation recognition (Baker and Cheng, 1996) is the method of choice. It proceeds iteratively: a model is used to generate projections in all possible directions and these projections are used to sort the original images by "supervised classification." An improved model is then calculated, and this procedure is repeated exhaustively. However, to get started, one needs an unbiased model of sufficient resolution and discriminatory power.

Originally, orientations were determined by the "common-lines" method (Crowther, 1971; Fuller, 1987; Baker *et al.*, 1988). Common lines are lines in the Fourier transform of an image of a symmetric particle, along which the values should be identical—at least for ideal, noise-free, data. Icosahedral symme-

[1] Current address: Centro Nacional de Biotecnología, Unidad de Microscopía Electrónica, Campus Universidad Autónoma, Cantoblanco 28049 Madrid, Spain.

[2] To whom correspondence should be addressed at Building 12A, Room 2033, MSC 5624, NIH, Bethesda, MD 20892-5624. Fax: (301) 402-2867. E-mail: TRUS@helix.nih.gov.

1047-8477/99

try provides 37 pairs of common lines for a single particle. "Cross common lines" relate lines in the transforms of different particles. In practice, on account of noise, one calculates residuals, defined as weighted sums of the discrepancies between all pairs of symmetry-related points. The most likely orientation is the one with the lowest residual. Common-lines has undergone further refinement (e.g., Thuman-Commike and Chiu, 1997; Böttcher *et al.*, 1997; Johnson *et al.*, 1994) but has been superceded in many studies by model-based methods. However, common-lines has an advantage that may be exploited in the early stages of analysis in that it is potentially capable of determining orientations from single images.

Here we outline a strategy for solving the structures of viruses that resist other methods. The key is to establish a small base set of correctly determined particles. These yield a first-generation reconstruction that is then fed into the model-based procedure. This approach evolved during our work on L-A—an RNA virus of yeast (Fig. 1; Caston *et al.*, 1997; Cheng *et al.*, 1994)—and has since been applied successfully to poliovirus (Belnap *et al.*, in preparation). Although related strategies have been developed independently by others (Baker and Cheng, 1996; Fuller *et al.*, 1996; Wikoff *et al.*, 1997), none has been described in detail and we present this report in the hope that it may help others tackling similar problems.

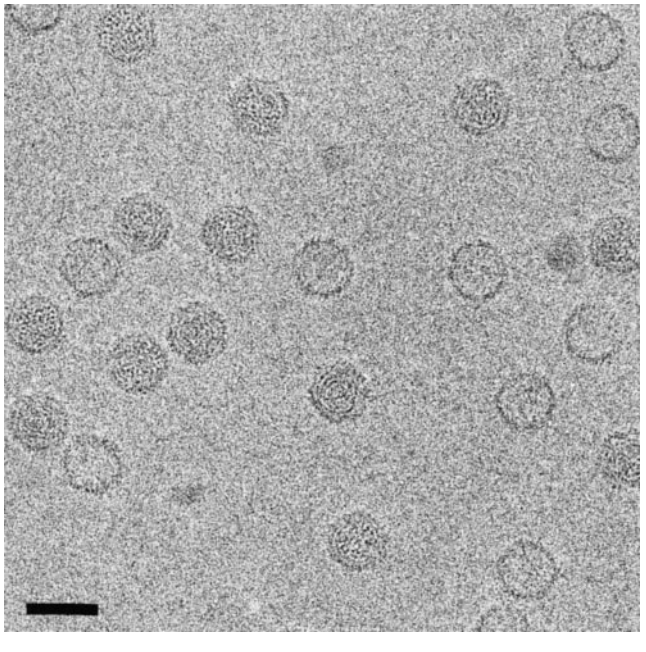

FIG. 1. Cryo-electron micrograph of purified L-A viral particles. Empty and RNA-filled particles are clearly distinguished: neither particle exhibits conspicuous features in these projections, even though the defocus (~1.67 μm, corresponding to a first zero of the contrast transfer function at $(25\ \text{Å})^{-1}$)) is such as to strongly convey frequencies typical of spacings between protein subunits. Bar, 500 Å.

STRATEGY

Our method involves five steps: selecting a small set of images for detailed analysis; determining possible orientations by common lines; calculating single-particle reconstructions (SPRs) for each orientation; evaluating the SPRs by comparing their reprojections to the original images; and evaluating multiparticle reconstructions in the same way.

1. Select a Small Set of Promising Particles

Pick out a few (e.g., 5–10) particles that exhibit relatively pronounced features that may be used to discriminate between candidate orientations. Such features are often most evident around the periphery. Determine the centers for particles.

2. Determine Possible Orientations

Run a common-lines program (e.g., Fuller *et al.*, 1996) to find candidate orientations for each particle. We typically keep the 25 solutions with the lowest self-residuals. This "best list" may be reduced by eliminating redundant solutions, i.e., orientations that differ by only 2–3°.

3. Calculate Single-Particle Reconstructions

Each candidate orientation is used to compute a SPR. We compute SPRs at low resolution (e.g., 40–50 Å); even so, they are usually very noisy. Noise may be reduced somewhat by "unblobbing" (Conway *et al.*, 1996) or by setting to background, all densities inside and/or outside a certain radius.

4. Compare Reprojections of SPRs to the Original Images

SPRs may be used to screen candidate orientations by visual evaluation. It is often possible to eliminate some candidates and to promote others by visual comparison between SPR reprojections and the original images, suitably band-limited (Fig. 2). To rank the surviving candidates, each SPR is projected according to its input orientation and then compared to the original cryo-EM image by cross-correlation (see Eq. (1)). The orientation with the highest correlation coefficient (CC) is taken as the best orientation for that particle. The comparison may be confined to its periphery, which often contains relatively pronounced features and where the signal from the edge of the particle is strong.

$$\mathrm{CC} = \frac{\Sigma_i p_i q_i}{\Sigma_i \{p_i^2\}^{1/2}\, \Sigma_i \{q_i^2\}^{1/2}}, \qquad (1)$$

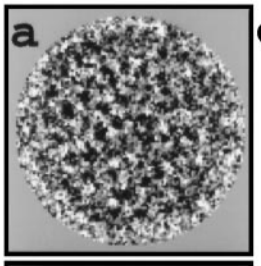

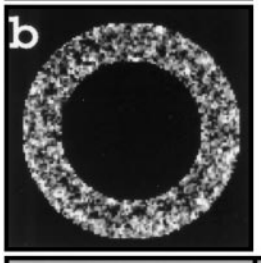

c

θ	ϕ	ω	residual-FV	CC_1	CC_2
73.0,	-1.0,	134.0	32.5 (1)	0.563 (3)	0.555 (3)
87.0,	2.0,	132.0	35.6 (4)	0.556 (4)	0.532 (7)
78.0,	7.0,	168.0	37.5 (5)	0.555 (5)	0.528 (8)
77.0,	-1.0,	131.0	39.5 (8)	0.554 (6)	0.541 (6)
80.0,	-7.0,	99.0	40.2 (10)	0.572 (1)	0.556 (2)
78.0,	-8.0,	98.0	40.8 (11)	0.482 (11)	0.523 (10)
78.0,	-6.0,	99.0	47.4 (18)	0.517 (10)	0.524 (9)
84.0,	11.0,	36.0	47.5 (19)	0.540 (7)	0.548 (5)
76.0,	-9.0,	99.0	49.3 (22)	0.533 (8)	0.551 (4)
80.0,	11.0,	25.0	49.6 (23)	0.527 (9)	0.497 (11)
78.0,	3.0,	112.0	49.9 (25)	0.568 (2)	0.572 (1)

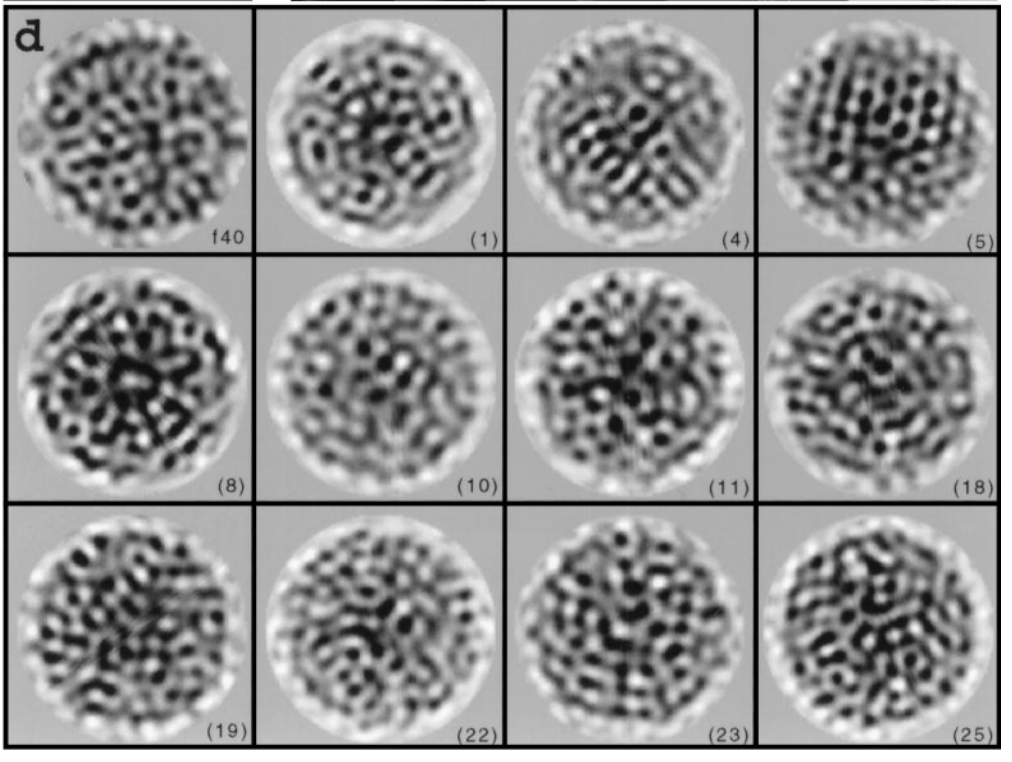

FIG. 2. Analysis of candidate orientations for an image of a L-A virion, shown in (a). (b) The same particle after imposing an annular mask. (c) A list of candidate orientations generated by the common-lines program, FINDVIEW. The orientations are defined by their Euler angles (θ, ϕ, and ω). The numbers given in parentheses in the fourth (residual) column show the ranking of each orientation in the "best list," according to its phase residual, given in degrees. (The original list of 25 was reduced to 11 by eliminating redundant solutions.) These numbers are used to label the corresponding reprojections in (d). Columns CC_1 and CC_2 list the correlation coefficients obtained for each reprojection with the masked (b) and unmasked (a) images, respectively. Rankings by this criterion are shown in parentheses for each column. (d) Shown at the top left is the particle image from (a) after low-pass filtering at $(40\ \text{Å})^{-1}$; the remaining images represent reprojections of the corresponding SPRs. Upon close visual inspection, it emerges that some candidates (e.g., (5), (11), (18), and (23)) project hexagonal profiles in significantly different orientations from the original image (a) and may thus be eliminated. Others show pronounced features (like the striations in (8) or the round-as-opposed-to-hexagonal profile of (1), (4), (10), and (22)) that are not shared by the original image (a, d) and may be rejected for that reason. In terms of both correlation coefficients (last two columns—cf. Eq. (1)), solutions (10) and (25) are favored, of which solution (25) eventually prevailed.

where p_i is the reprojection image, and q_i is the raw filtered image.

5. Calculate and Evaluate Multiparticle Reconstructions (MPRs)

At this point, the only way to further reduce the noise level in the SPR is to combine particles. Accordingly, calculate MPRs from two or more particles, starting with combinations of candidate orientations that appear most likely. MPRs should be evaluated by the same criteria as SPRs, in particular, visual and correlation-based comparison of reprojections with the original, band-limited images.

Once a base set is established, it is fed into a standard application of model-based refinement (Baker and Cheng, 1996), progressively drawing in more particles and allowing increasingly precise angular refinement. For capsids in the range of 30–45 nm in diameter, five or six particles should suffice for a base set.

Criteria for Correct and Incorrect Solutions

How does one know that a given SPR or MPR is correct? This is a difficult question: in practice, it is hard to completely exorcise intuition, but the following guidelines may help. If, on visually comparing surface renderings, one SPR of particle A resembles one SPR of particle B, both orientations may be correct since at most one solution in each best list is right. SPRs that depict very smooth, near-spherical particles should be treated with caution. Base set particles should remain stable with one solution and not vacillate between two or more solutions. Adding a particle to a current data set should produce an overall increase in the correlation coefficients if the newcomer's orientation is correct. Moreover, the resolution of the resulting MPR should improve (Saxton and Baumeister, 1982; Conway *et al.*, 1993). Also, the structure visualized should also be consistent with any *a priori* information that is available, such as copy number (or triangulation number—Caspar and Klug, 1962) or the oligomeric nature of the capsomers.

A Case History

A cryo-micrograph of L-A virions is shown in Fig. 1. A set of empty particles was selected and a common-lines list of the 25 most likely solutions was obtained for each. After redundant solutions were eliminated, the corresponding SPRs were calculated to 40-Å resolution and unblobbed. The candidates were then evaluated, as illustrated for one particle in Figs. 2 and 3. Some orientations (e.g., Nos. 5, 8, and 11) may be eliminated on grounds of evident visual inconsistency between the SPR reprojection and the original image (cf. Fig. 2d). The remaining candidates were ranked in terms of their correlation coefficients (Fig. 2c). Although correlation coefficients have limitations—e.g., they may vary only slightly in value over a set that includes both correctly and incorrectly identified particles—it has been our experience that solutions that rank high for both correlation coefficients (total and annular) are often correct. In this case, there are two such solutions, Nos. 10 and 25. Of these, No. 25 seems to be a better visual match and subsequent analysis indicated that it was indeed the correct solution. None of the 11 candidate SPRs is obviously correct or incorrect from visual inspection of their surface renderings (Fig. 3).

The correct relative handedness of particles whose orientation angles have been established remains to be determined (for determination of absolute handedness, see (Belnap *et al.*, 1997)). In the convention used here, there are two possible enantiomorphs corresponding to values of ω and $\omega + 180°$, respectively, for the third Euler angle. Fixing the first image, a second image may be combined with it with either handedness (two solutions). Our strategy is to establish consistent handedness for a manageably small set of particles by calculating a MPR for each permutation of handedness (e.g., eight such MPRs with four particles) and to evaluate them as described above. A comparison of three raw images with their correct SPR reprojections and reprojections from the final MPR model illustrates their mutual consistency (Fig. 4). Combining particles with inconsistent handedness leads to an artifactual symmetrization, a general smoothing, and a loss of dynamic power. After enough particles have been incorporated with consistent handedness to give an MPR with sufficient resolution, it may be relied upon to solve additional particles with consistent handedness as the data set is expanded via the model-based approach.

DISCUSSION

We have outlined a procedure for determining the orientations of refractory virus particles (e.g., capsids with smooth surfaces, roundish profiles, and filled interiors). Using it, we were able to solve two viruses that resisted solution by other means: L-A (Caston *et al.*, 1997; Cheng *et al.*, 1994) and poliovirus (Belnap *et al.*, in preparation). We wished to solve the latter virus *de novo* from cryo-micrographs, even though a high-resolution crystallographic structure was available (Hogle *et al.*, 1985). It was solved

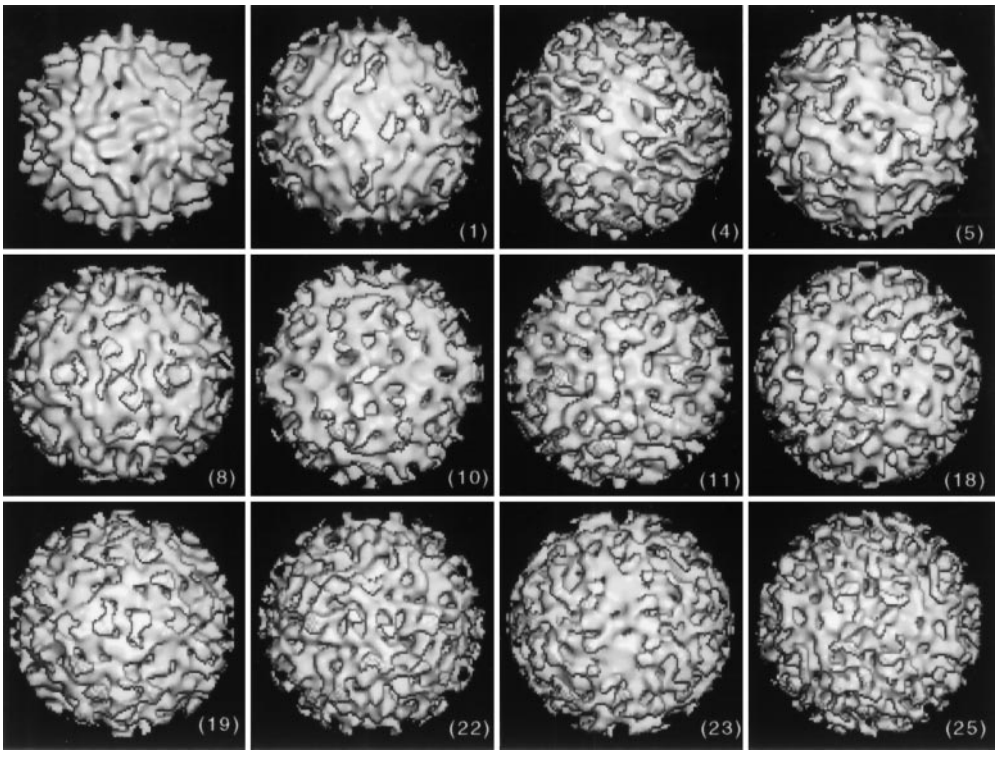

FIG. 3. Surface renderings of 11 SPRs, each corresponding to a candidate orientation for the trial particle (as listed in Fig. 2c), are compared to that of the final, well-defined, density map (top left). Because of their high noise level, these images give no clear indication as to which, if any, SPR corresponds to the correct orientation. In this respect, the corresponding reprojections from the SPRs proved to be informative (see Fig. 2).

as outlined above: a two-particle reconstruction calculated to 39-Å resolution led, after numerous cycles of model-based refinement, to a final 120-particle reconstruction at 22-Å resolution.

Use of SPRs was first reported by Fuller and colleagues (Dokland *et al.,* 1992; Venien-Bryan and Fuller, 1994; Fuller *et al.,* 1996). It has been our experience that reprojections are more useful than surface renderings for evaluation of SPRs (cf. Figs. 2 and 3) and we are not aware of them having been used before. For larger viruses, the Fourier–Bessel reconstruction method (Crowther, 1971) may not allow SPRs to be calculated to resolutions high enough to allow evaluation, although such SPRs (albeit noisy) can be calculated by back-projection (Radermacher, 1992).

Because it depends on the high order of symmetry of icosahedral particles, which makes it possible to calculate SPRs, the strategy described here does not adapt readily to the analysis of particles with lower symmetries. Nevertheless, some other approaches are possible and have in common the principle of seeking to enhance the signal or reduce the noise in the data set:

(1) The S:N ratio may be enhanced by image restorations that combine focal pairs or triplets (Conway *et al.,* 1997; Trus *et al.,* 1997), thus expanding the range of frequencies that are strongly conveyed. In marginal cases, the resulting improvement may be enough to render the data solvable.

(2) Labeling particles with antibody fragments or other bulky ligands will enhance the surface relief, so that the various projections are more strongly differentiated and may be recognized more easily and with greater precision.

(3) Tomographic reconstructions (Walz *et al.,* 1998) produce density maps of individual particles of any symmetry, although they are limited in resolution by the total electron dose. Such reconstructions, enhanced by aligning and averaging, should serve as a valuable source of starting models (Walz *et al.,* 1997).

(4) Negative staining (Kolodziej *et al.,* 1997), perhaps combined with low-temperature techniques (Adrian *et al.,* 1998), provides specimens with higher contrast and greater radiation resistance that may also serve as a source of starting models for reconstructing cryo-electron micrographs.

(5) Angular reconstitution (van Heel, 1987) affords another approach. In this case, the S:N is boosted by class averaging after multivariate statistical analysis. This is a powerful method, although

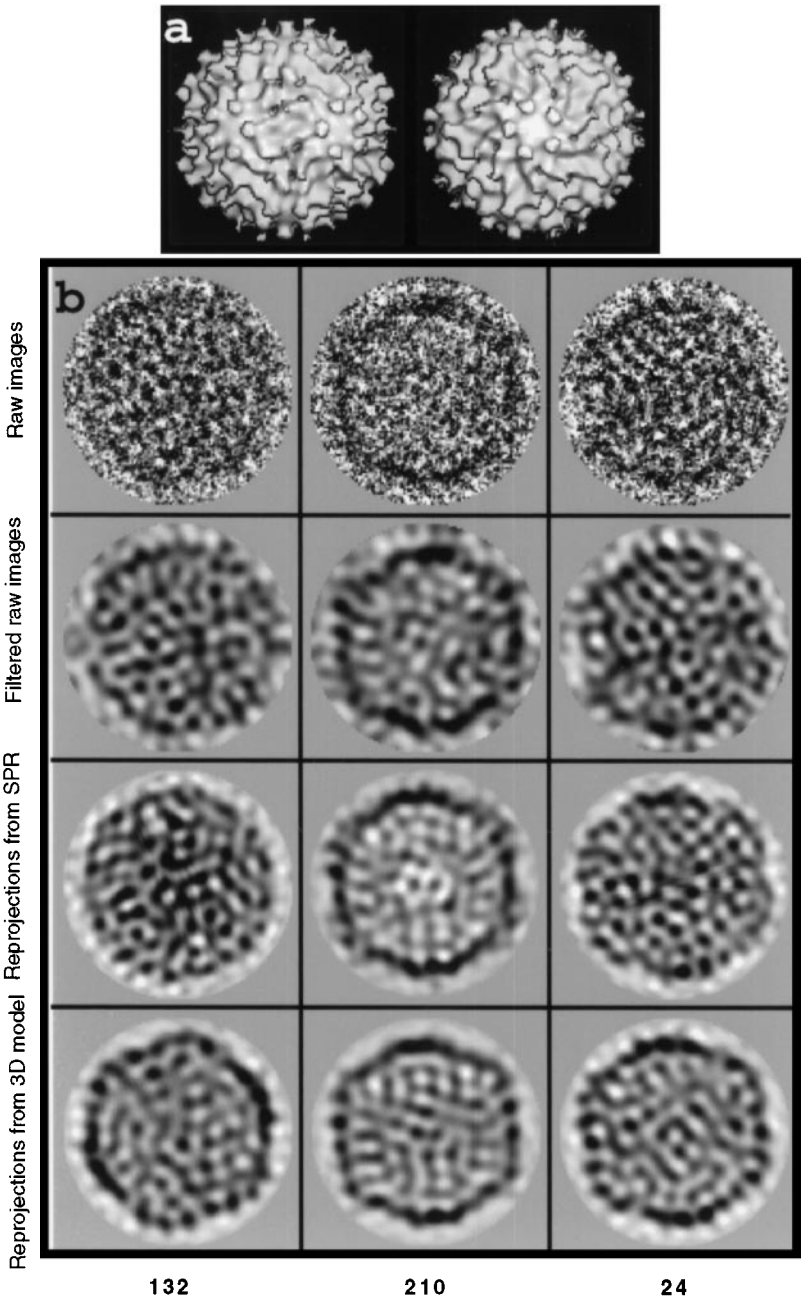

FIG. 4. Steps in the calculation of an MPR of L-A virus made according to the procedure described. (a) Outer surface of a 3PR computed from particles 132, 210, and 24. The views are along twofold (left) and fivefold (right) symmetry axes. (b) First row, original images; and second row, band-limited images obtained after low-pass filtering at $(40\ \text{Å})^{-1}$. Reprojections of their SPRs in the assumed viewing orientations (third row) are compared to reprojections (fourth row) obtained from the 3PR shown in (a).

its applicability depends, to some extent, on the particle presenting a limited number of preferential views and having enough structural irregularity to generate images for which reliable classification is possible.

It is not evident to us that any single method is universally optimal. Rather, each kind of particle is likely to be most amenable to some particular strategy or combination of strategies. As the above list illustrates, there is a fertile range of possible approaches. In three-dimensional analysis of single particles, accurate and precise determination of orientations represents what is often technically the most challenging phase of the analysis.

We thank Dr. James Conway for helpful discussions, Dr. Tim Baker for critically reading the manuscript, and Dr. Reed Wickner for preparations of L-A virions.

REFERENCES

Adrian, M., Dubochet, J., Lepault, J., and McDowall, A. W. (1984) Cryo-electron microscopy of viruses, *Nature* **308,** 32–36.

Adrian, M., Dubochet, J., Fuller, S. D., and Harris, J. R. (1998) Cryo-negative staining, *Micron* **29,** 145–160.

Baker, T. S. (1992) Cryo-electron microscopy and three-dimensional image reconstruction of icosahedral viruses. *In* Megías-Megías, L., Rodríquez-García, M. I., Ríos, A., and Arias, J. M. (Eds.), Electron Microscopy 92: Proceedings of the 10th European Congress on Electron Microscopy, Granada, Spain, 7–11 September 1992, Vol. 3, pp. 275–279, Secretairado de Publicaciones de la Universidad de Granada, Granada.

Baker, T. S., and Cheng, R. H. (1996) A model-based approach for determining orientations of biological macromolecules images by cryoelectron microscopy, *J. Struct. Biol.* **116,** 120–130.

Baker, T. S., Drak, J., and Bina, M. (1988) Reconstruction of three-dimensional structure of simian virus 40 and visualization of the chromatin core, *Proc. Natl. Acad. Sci. USA* **85,** 422–426.

Baker, T. S., and Johnson, J. E. (1997) Principles of virus structure determination, *in* Chiu, W., Burnett, R. M., and Garcea, R. L. (Eds.), Structural Biology of Viruses, pp. 38–79, Oxford Univ. Press, New York.

Belnap, D. M., Olson, N. H., and Baker, T. S. (1997) A method for establishing the handedness of biological macromolecules, *J. Struct. Biol.* **120,** 44–51.

Böttcher, B., Wynne, S. A., and Crowther, R. A. (1997) Determination of the fold of the core protein of hepatitis B virus by electron cryomicroscopy, *Nature* **386,** 88–91.

Caspar, D. L. D., and Klug, A. (1962) Physical principles in the construction of regular viruses, *Cold Spring Harbor Symp. Quant. Biol.* **27,** 1–24.

Caston, J. R., Trus, B. L., Booy, F. P., Wickner, R. B., Wall, J. S., and Steven, A. C. (1997) Structure of L-A virus: A specialized compartment for the transcription and replication of double-stranded RNA, *J. Cell. Biol.* **138,** 975–985.

Cheng, R. H., Caston, J. R., Wang, G., Gu, F., Smith, T. J., Baker, T. S., Bozarth, R. F., Trus, B. L., Cheng, N., Wickner, R. B., and Steven, A. C. (1994) Fungal virus capsids, cytoplasmic compartments for the replication of double-stranded RNA, formed as icosahedral shells of asymmetric Gag dimers, *J. Mol. Biol.* **244,** 255–258.

Chiu, W. (1993) What does electron cryomicroscopy provide that X-ray crystallography and NMR spectroscopy cannot? *Ann. Rev. Biophys. Biomol. Struct.* **22,** 233–255.

Conway, J. F., Trus, B. L., Booy, F. P., Newcomb, W. W., Brown, J. C., and Steven, A. C. (1993) The effects of radiation damage on the structure of frozen hydrated HSV-1 capsids, *J. Struct. Biol.* **111,** 222–233.

Conway, J. F., Trus, B. L., Booy, F. P., Newcomb, W. W., Brown, J. C., and Steven, A. C. (1996) Visualization of three-dimensional density maps reconstructed from cryoelectron micrographs of viral capsids, *J. Struct. Biol.* **116,** 200–208.

Conway, J. F., Cheng, N., Zlotnick, A., Wingfield, P. T., Stahl, S. J., and Steven, A. C. (1997) Visualization of a 4-helix bundle in the hepatitis B virus capsid by cryo-electron microscopy, *Nature* **386,** 91–94.

Crowther, R. A. (1971) Procedures for three-dimensional reconstruction of spherical viruses by Fourier synthesis from electron micrographs, *Philos. Trans. R. Soc. Lond. B* **261,** 221–230.

Dokland, T., Lindqvist, B. H., and Fuller, S. D. (1992) Image reconstruction from cryo-electron micrographs reveals the morphopoietic mechanism in the P2–P4 bacteriophage system, *EMBO J.* **11,** 839–846.

Fuller, S. D. (1987) The T = 4 envelope of Sindbis virus is organized by interactions with a complementary T = 3 capsid, *Cell* **48,** 923–934.

Fuller, S. D., Butcher, S. J., Cheng, R. H., and Baker, T. S. (1996) Three-dimensional reconstruction of icosahedral particles—The uncommon line, *J. Struct. Biol.* **116,** 48–55.

Hogle, J. M., Chow, M., and Filman, D. J. (1985) Three-dimensional structure of poliovirus at 2.9 Å resolution, *Science* **229,** 1358–1365.

Johnson, C. A., Weisenfeld, N. I., Trus, B. L., Conway, J. F., Martino, R. L., and Steven, A. C. (1994) Orientation determination in the 3D reconstruction of icosahedral viruses using a parallel computer. *in* Proceedings, Supercomputing, pp. 550–559, IEEE Computer Society Press, Los Alamitos, CA.

Kolodziej, S. J., Penczek, P. A., and Stoops, J. K. (1997) Utility of butvar support film and methylamine tungstate stain in three-dimensional electron microscopy: Agreement between stain and frozen-hydrated reconstructions, *J. Struct. Biol.* **120,** 158–167.

Radermacher, M. (1992) Weighted back-projection methods. *in* Frank, J. (Ed.), Electron Tomography—Three-Dimensional Imaging with the Transmission Electron Microscope, pp. 91–116. Plenum, New York.

Saxton, W. O., and Baumeister, W. (1982) The correlation averaging of a regularly arranged bacterial cell envelope protein, *J. Microsc.* **127,** 127–138.

Thuman-Commike, P. A., and Chiu, W. (1997) Improved common line-based icosahedral particle image orientation estimation algorithms, *Ultramicroscopy* **68,** 231–255.

Trus, B. L., Roden, R. B. S., Greenstone, H. L., Vrhel, M., Schiller, J. T., and Booy, F. P. (1997) Novel structural features of bovine papillomavirus capsid revealed by three dimensional reconstruction to 9Å resolution, *Nat. Struct. Biol.* **4,** 413–420.

van Heel, M. (1987) Angular reconstitution: A posteriori assignment of projection directions for 3D reconstructions, *Ultramicroscopy* **21,** 111–124.

Venien-Bryan, C., and Fuller, S. D. (1994) The organization of the spike complex of Semliki forest virus, *J. Mol. Biol.* **236,** 572–583.

Walz, J., Tamura, T., Tamura, N., Grimm, R., Baumeister, W., and Koster, A. J. (1997) Tricorn protease exists as an icosahedral supermolecule in vivo, *Mol. Cell* **1,** 59–65.

Walz, J., Typke, D., Nitsch, M., Koster, A., Hegerl, R., and Baumeister, W. (1998) Electron tomography of single ice-embedded macromolecules: Three dimensional alignment and classification, *J. Struct. Biol.* **120,** 387–396.

Wikoff, W. R., Tsai, C. J., Wang, G., Baker, T. S., and Johnson, J. E. (1997) The structure of cucumber mosaic virus: Cryoelectron microscopy, X-ray crystallography, and sequence analysis, *Virology* **232,** 91–97.